Closed Loop Light Beam Micromanipulators for Optical Metrology

L. Ngo Phong, J. Lee, I. Ressejac, M. Maszkiewicz, and W. Zheng
Canadian Space Agency
Saint-Hubert, Quebec, Canada

S. Crisan, L. Le Noc, F. Picard, and H. Jerominek
INO
Sainte-Foy, Quebec, Canada

Abstract

The use of light beam micromanipulators in space subsystems has received particular attention in recent years. To compensate for changes in system parameters during the flight, these devices require closed loop control. This paper reports on an integrated feedback mechanism devised for flexural tortional devices. It consists in using monolithically embedded photodetectors to measure the portion of incident light crossing an aperture created in the manipulator. The manipulator position is determined from the detector section shadowed by the displaced aperture. A model is presented for the electrostatically actuated manipulator, predicting effects of structural parameters on angular displacement and resolution. As proof of concept, photodiode assisted closed loop manipulators were microfabricated in varying configurations on Si wafer. Their characteristics of deflection versus actuation voltage were better than those predicted by the model. The feedback mechanism was validated in light of the good agreement between differential photocurrents measured from contiguous photodiodes and theoretical prediction. Details on device modeling, microfabrication, and characterization are reported.

1. Introduction

Today's trend in distributing the functionality of large spacecraft among smaller, cheaper, cooperative spacecraft has created the need for formation flight control and collision avoidance. This is the motivation behind developing metrology subsystem for miniature spacecraft to determine relative distances and orientations of its partners. Such a system finds use also in operations such as spacecraft rendez-vous and docking. At orbits where access to GPS data is unavailable or undependable, metrology has to be achieved autonomously by either rf or optical measurement. The former is less suited for miniature spacecrafts because of the extended baseline required for rf interferometry and relatively high power consumption [1]. Optical metrology, on the other hand, is free of these constraints and immune to electromagnetic interference. One technique employed in optical metrology consists in steering a modulated or pulsed laser beam towards the retroreflector on partner spacecraft and measuring the travel time of reflected beam. The beam steering makes use habitually of electrostatic [2], electromagnetic [3], or piezoelectric [1] light beam manipulators. Because electrostatic actuation involves charging and discharging of small capacitors, the power consumed is small, making it easier to implement than counterparts [2]. However, most electrostatically actuated manipulators consist so far of open loop devices in which predetermined input-output relations govern the amount of displacement for a driving signal. For space applications the open loop approach is inadequate because system parameters may change with time and environment disturbance. One method to achieve closed loop control is to integrate position feedback sensor with the manipulator. This way, upon receiving feedback on the manipulator position, command signals can be adjusted in real time to compensate for changes in system parameters.

This paper reports on a feedback mechanism devised for closed loop control of manipulators. This mechanism, assisted by the use of photodetector arrays, has been implemented and demonstrated in electrostatically actuated flexural tortional devices. In the following the device configuration and modeling results will first be presented. After this, details of the device microfabrication and characteristics will be reported.

2. Device configuration

Figure 1 shows the schematic of a closed loop micromanipulator. The device consists of an Al alloy cantilever structure incorporating a reflective Al film. This structure is anchored to the Si wafer via a beam that can electrostatically be deflected in flexural-tortional mode. Actuation voltages are supplied to a pair of electrodes located under the structure. If voltages are equally supplied to the electrodes, deflection is only flexural. Otherwise, an added tortional deflection will occur. Two square apertures are created in the structure to allow the underside photodetectors to collect a portion of the light incident on the structure. When the structure is deflected, the resulting misalignment between aperture and detector is such that a fraction of detector area is shadowed by the structure. This

0-7695-2189-4/04 $20.00 © 2004 IEEE

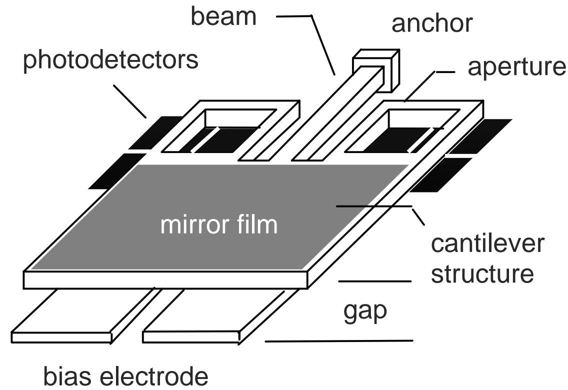

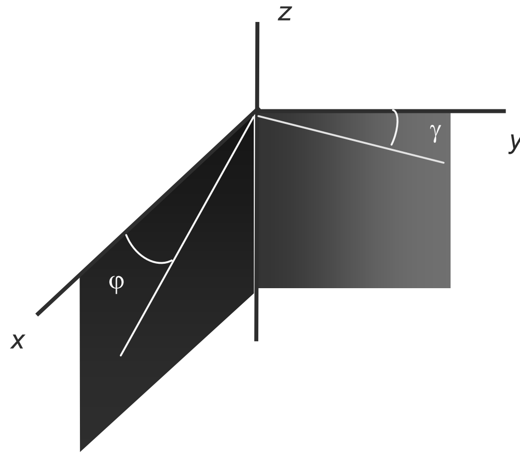

Fig. 1 – Schematic of a photodetector assisted closed loop micromanipulator with flexural angle φ and tortional angle γ

occurrence is illustrated in Fig. 2 for the case of flexural deflection. Feedback on manipulator position is obtained by monitoring the shadowed fraction of detector area.

3. Modeling results

To assist in the design of the micromanipulator, modeling has been used to predict the effects of structural parameters on angular displacement for a given bias voltage. Modeling was performed both analytically and using finite element technique. Analytically, we expanded the model presented by Toshiyoshi and Fujita [4] for electrostatic torsional mirrors to further include the flexural actuation and flexural tortional coupling. Depending upon the values of bias voltages on the pair of electrodes, V_1 and V_2, one of the following deflection modes would occur:

- flexural deflection: $V_1 = V_2$;

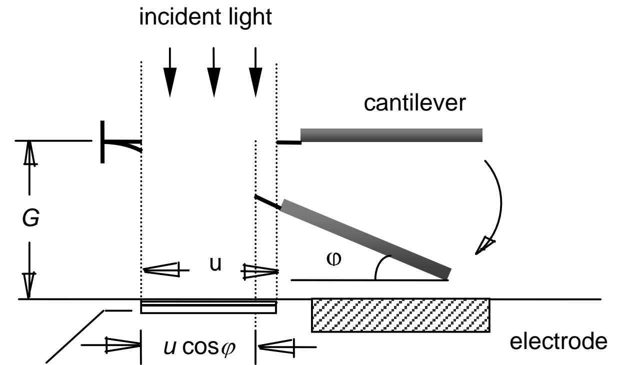

Fig. 2 – Side view of a flexural cantilever structure with aperture size *u* above the underside photodetectors

- torsional deflection: $V_1 = -C(\gamma)\, V_2$, where the positive parameter $C(\gamma)$ is a function of torsional angle γ; and
- combined flexural torsional deflection.

The analytical treatment of the general case, *i.e*. combined flexural torsional deflection, is presented hereafter with following assumptions:

- the length (*x*-axis) and width (*y*-axis) of each electrode correspond respectively to the length and half-width of the mirror film;
- deflection occurs solely at the beam, the remaining of the structure is not deformed; and
- flexural angle φ and torsional angle γ are both small.

The approach used in the treatment consists in comparing the expression for the beam's electrostatic moment, which contains the bias voltage term, with the one for the beam's restoring torque, which includes the deflection angle term. The structural parameters used in the treatment are defined in Figs 3 and 4 respectively for flexural and tortional deflection modes. By convention, the value of φ is positive when the structure bends downward, and that of γ is positive when structure rotates clockwise as viewed from free end.

Upon applying a bias voltage, *V*, to the electrode, the magnitude of the electrostatic force, *F*, exerted on an incremental area d*x*d*y* of the structure is expressed as:

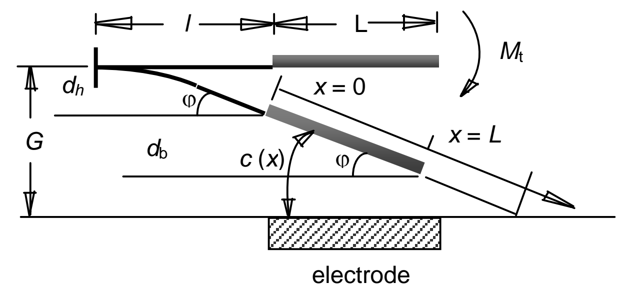

Fig. 3 – Side view of a flexural cantilever structure

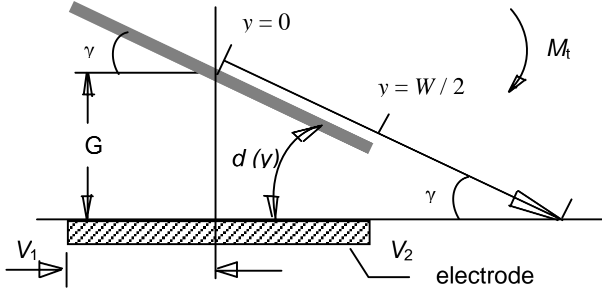

Fig. 4 - Front view of a torsional cantilever structure

$$dF = \frac{1}{2}\varepsilon_0 dxdy \frac{V^2(y)}{d^2(x,y)}$$

where:

$$V(y) = \begin{cases} V_1 & \text{for } y \in [-\frac{W}{2},0] \\ V_2 & \text{for } y \in [0,\frac{W}{2}] \end{cases}$$

$$d(x,y) = (\frac{G-d_h}{\sin\varphi} - x)\varphi - y\gamma$$

As a result, the overall flexural moment ($M = x\mathrm{d}F$) with respect to the y-axis is:

$$M_e = M_1 + M_2$$

with M_1 and M_2 being the components respectively due to the voltages V_1 and V_2 supplied to the two electrodes,

$$M_1 = \int_0^L \int_{-W/2}^0 \frac{1}{2}\varepsilon_0 \frac{V_1^2}{(\frac{G-d_h}{\sin\varphi}\varphi - x\varphi - y\gamma)^2} x\mathrm{d}x\mathrm{d}y$$

$$M_2 = \int_0^L \int_0^{W/2} \frac{1}{2}\varepsilon_0 \frac{V_2^2}{(\frac{G-d_h}{\sin\varphi}\varphi - x\varphi - y\gamma)^2} x\mathrm{d}x\mathrm{d}y$$

For small values of φ, one obtains:

$$M_1 = \frac{\varepsilon_0 V_1^2}{2\varphi^2\gamma} \cdot [(G-d_h)\ln\frac{G-d_h}{G-d_h-L\varphi} + (G-d_h+\frac{1}{2}W\gamma)\ln\frac{G-d_h-L\varphi+\frac{1}{2}W\gamma}{G-d_h+\frac{1}{2}W\gamma}]$$

$$M_2 = \frac{\varepsilon_0 V_2^2}{2\varphi^2\gamma} \cdot [(G-d_h-\frac{1}{2}W\gamma)\ln\frac{G-d_h-\frac{1}{2}W\gamma}{G-d_h-L\varphi-\frac{1}{2}W\gamma} + (G-d_h)\ln\frac{G-d_h-L\varphi}{G-d_h}]$$

At equilibrium, the flexural moment M_e equals the restoring moment M_s of the beam (length l, width w_h, thickness t_h, Young's module E). The expressions for M_s and deflection, d_h, are as follows for anchored cantilever beam:

$$M_s = \frac{EI}{l}\varphi$$

$$|d_h| = \frac{M_s l^2}{2EI} = \frac{1}{2}\varphi\, l$$

where I is the moment of inertia of the beam's cross section:

$$I = w_h\, t_h^3 / 12$$

Equalizing M_e to M_s yields:

$$B_1(\varphi,\gamma)V_1^2 + B_2(\varphi,\gamma)V_2^2 = \frac{2EI}{\varepsilon_0 l}\varphi^3\gamma \tag{1}$$

where:

$$\begin{cases} B_1(\varphi,\gamma) = (G-d_h)\ln\frac{G-d_h}{G-d_h-L\varphi} + (G-d_h+\frac{1}{2}W\gamma)\ln\frac{G-d_h-L\varphi+\frac{1}{2}W\gamma}{G-d_h+\frac{1}{2}W\gamma} \\ B_2(\varphi,\gamma) = (G-d_h-\frac{1}{2}W\gamma)\ln\frac{G-d_h-\frac{1}{2}W\gamma}{G-d_h-L\varphi-\frac{1}{2}W\gamma} + (G-d_h)\ln\frac{G-d_h-L\varphi}{G-d_h} \end{cases}$$

The tortional component is also derived using the above approach. For an incremental area $\mathrm{d}x\mathrm{d}y$, the torque resulted from the applied electrostatic force is:

$$dT = ydF_e = \frac{1}{2}\varepsilon_0 y\mathrm{d}x\mathrm{d}y \frac{V^2(y)}{d^2(x,y)}$$

and the overall torque due to V_1 and V_2 is:

$$T_e = T_1 + T_2$$

where:

$$T_1 = \int_0^L \int_{-W/2}^{0} \frac{1}{2} \varepsilon_0 \frac{V_1^2}{(\frac{G-d_h}{\sin\varphi}\varphi - x\varphi - y\gamma)^2} y\mathrm{d}x\mathrm{d}y$$

$$T_2 = \int_0^L \int_0^{W/2} \frac{1}{2} \varepsilon_0 \frac{V_2^2}{(\frac{G-d_h}{\sin\varphi}\varphi - x\varphi - y\gamma)^2} y\mathrm{d}x\mathrm{d}y$$

For small values of γ, one obtains:

$$T_1 = \frac{\varepsilon_0 V_1^2}{2\gamma^2\varphi} \cdot [(G-d_h)\ln\frac{G-d_h}{G-d_h+\frac{1}{2}W\gamma} + (G-d_h-L\varphi)\ln\frac{G-d_h-L\varphi+\frac{1}{2}W\gamma}{G-d_h-L\varphi}]$$

$$T_2 = \frac{\varepsilon_0 V_2^2}{2\gamma^2\varphi} \cdot [(G-d_h)\ln\frac{G-d_h-\frac{1}{2}W\gamma}{G-d_h} + (G-d_h-L\varphi)\ln\frac{G-d_h-L\varphi}{G-d_h-L\varphi-\frac{1}{2}W\gamma}]$$

At the same time, the restoring torque of the beam is expressed as:

$$T_t = \frac{G_n J_n}{l}\gamma$$

where G_n and J_n are respectively the shear modulus and shear moment of inertia of the beam,

$$G_n = \frac{E}{2(1+\mu)}, \qquad J_n = \beta w_h t_h^3$$

μ is the Poisson ration and

$$\beta = \frac{1}{3} \quad \text{for} \quad \frac{w_h}{t_h} > 10$$

At equilibrium $T_e = T_t$ and it follows that:

$$C_1(\varphi,\gamma)V_1^2 + C_2(\varphi,\gamma)V_2^2 = 2\frac{G_n J_n}{\varepsilon_0 l}\gamma^3\varphi \qquad (2)$$

where:

$$\begin{cases} C_1(\varphi,\gamma) = (G-d_h)\ln\dfrac{G-d_h}{G-d_h+\frac{1}{2}W\gamma} + (G-d_h-L\varphi)\ln\dfrac{G-d_h-L\varphi+\frac{1}{2}W\gamma}{G-d_h-L\varphi} \\ C_2(\varphi,\gamma) = (G-d_h)\ln\dfrac{G-d_h-\frac{1}{2}W\gamma}{G-d_h} + (G-d_h-L\varphi)\ln\dfrac{G-d_h-L\varphi}{G-d_h-L\varphi-\frac{1}{2}W\gamma} \end{cases}$$

Solving for V_1 and V_2 by combining Eqs. 1 and 2 for the flexural and torsion components, the equations describing the flexural tortional deflection are obtained as follows:

$$\begin{cases} V_1^2 = \dfrac{B_2 \cdot 2\frac{G_n J_n}{\varepsilon_0 l}\gamma^3\varphi - C_2 \cdot \frac{2EI}{\varepsilon_0 l}\varphi^3\gamma}{B_2 C_1 - B_1 C_2} \\ V_2^2 = \dfrac{C_1 \cdot \frac{2EI}{\varepsilon_0 l}\varphi^3\gamma - B_1 2\frac{G_n J_n}{\varepsilon_0 l}\gamma^3\varphi}{B_2 C_1 - B_1 C_2} \end{cases}$$

It should be noted that this set of equations does not account for the special case of purely flexural or torsion deflection. Treatments dedicated to such special cases were presented elsewhere [5]. Still, the results obtained from the general case's equations should border on those obtained from the special case's equations when either value of φ or γ is sufficiently small. Figure 5 shows the data computed for the case of flexural deflection for two different devices, whose parameters are presented in Table 1. It is seen that data obtained using general case's equations with γ set to be 0.01 deg are almost identical to those computed with special case's equations. For the larger one of the two devices, flexural deflection of ~ 3.5 deg is achieved with a bias voltage of ~ 37 V equally supplied to both electrodes.

To provide insight to the feedback sensitivity, we have examined the dependence on device parameters for the case of flexural devices. Referring to Fig. 2, it is seen that upon deflection the relative reduction in photoresponse can be expressed as the ratio of the shaded area, A_s, to the full active area, A, of the detector element:

$$\frac{A_s}{A} = \frac{(u/2)(u - u\cos\varphi)}{(u/2)^2} = 2(1-\cos\varphi)$$

Table 1 - Parameters of experimental light beam micromanipulators

	Device1	*Device 2*
Cantilever length L (μm)	80	100
Cantilever width W (μm)	70	200
Beam length l (μm)	80	100
Beam width w_h (μm)	10	10
Beam thickness t_h (μm)	1	1
Young's modulus (Al alloy) E (GPa)	70	70
Poisson ratio μ	0.34	0.34
Gap G (μm)	20	20

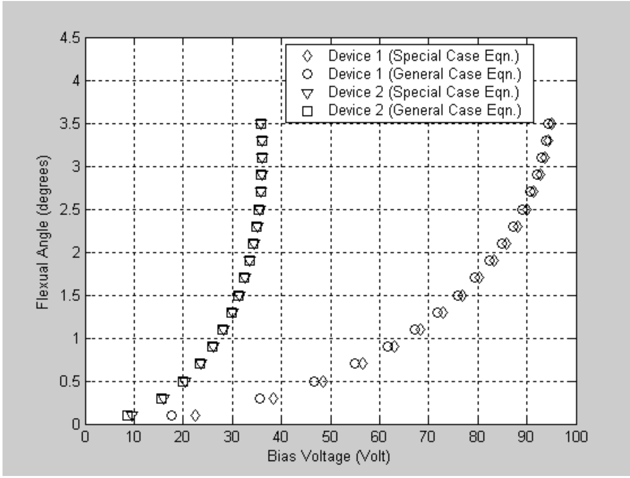

Fig. 5 – Bias voltage dependence of flexural angle as predicted by special case's equation and general case's equation with $\gamma = 0.01$ deg. Results are presented for two different devices whose parameters are provided in Table 1.

where u is the size of the aperture created in the structure. The resolution of the feedback mechanism is the angular displacement that induces a relative reduction in photoresponse equal to the noise to signal ratio, V_n / V, of the detector:

$$\frac{V_n}{V} = \frac{A_s}{A} = 2(1 - \cos\varphi)$$

Hence, the detectivity of the detector can be related to the feedback resolution as:

$$D^* = \frac{(\Delta f)^{1/2} V}{p A^{1/2} V_n} = \frac{(\Delta f)^{1/2}}{2 p A^{1/2} (1 - \cos\varphi)}$$

$$= \frac{(\Delta f)^{1/2}}{p u (1 - \cos\varphi)}$$

with p being the power density of incident light and Δf the measuring bandwidth of noise. Assuming for instance, Δf = 1 Hz, u = 100 μm, p = 500 mW / cm^2, D^* = 10^{10} cm.Hz$^{1/2}$/W, the resulting angular resolution is typically 0.01 deg. Higher resolutions can be achieved with the use of detectors with larger detectivities and larger active areas.

4. Microfabrication details

Experimental manipulators were micromachined in varying configurations on n-type (100) Si wafers. Details of the fabrication process are outlined in this section. The process comprises two main parts: (i) fabrication of photodiode elements by impurity diffusion; and (ii) fabrication of cantilever structures by Si surface micromachining. For a better understanding of the process flow, an illustration of the cross sectional schematic of the device is shown in Fig. 6. A 100-nm thick film of Si_3N_4 was first grown by PECVD on one side of the wafer, insulating it electrically from the metal electrodes. After this, windows were opened using an HF etch to remove Si_3N_4 at locations selected for the formation of photodiodes. To diffuse spun-on p-type dopant (Boron) in these windows, the wafer underwent a heat treatment at temperature ~ 1000 ^{o}C for 30 min. The resulting junction depth was estimated to exceed 400 nm under this condition. In the metallization step that followed, magnetron dc sputtering was used to deposit 300-nm thick Al film as electrodes and interconnects on insulating Si_3N_4. Al film was deposited also on the back side of the wafer to provide a common ground for the photodiodes. Once done, the photodiodes were passivated with magnetron sputtered SiO_2 film. To make use of the passivating film as an antireflective coating, the film thickness was monitored *in-situ* during deposition to be a multiple quarter wavelength of the incident light. Considering the HeNe laser source used in the experiment (wavelength ~ 633 nm), the film thickness was selected to be 319 nm (3λ/4). The passivating film was also used to insulate the electrodes where possible contact with the pull-in cantilever may occur. Following the formation of photodiodes, the wafer was spin coated with a 20-μm thick sacrificial polymide film which defined the gap between the cantilever and the electrode. The anchor of the cantilever structure was then

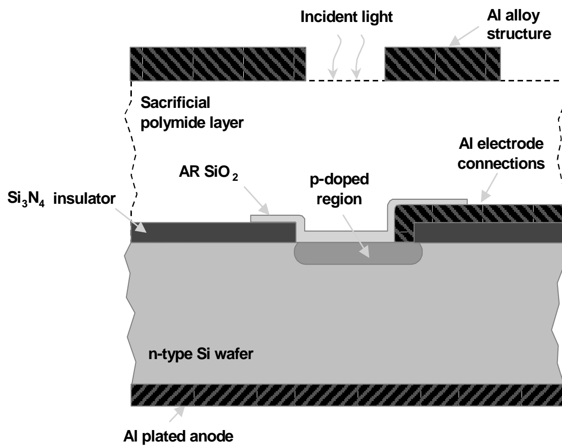

Fig. 6 – Cross sectional schematic of a light beam micromanipulator

formed in the sacrificial layer by O_2 plasma reactive ion etching. Finally, a 1-μm thick Al film was sputter deposited and patterned in a H_3PO_4 and HNO_3 solution to form the mirror part.

5. Experimental results

Figure 7 shows the scanning electron micrograph of an experimental light beam micromanipulator. The free standing cantilever structure is seen to be steadily anchored to the Si wafer and free of residual material. Unlike smaller structures that exhibit excellent planarity after release from sacrificial layer, most of the larger structures (such as the one shown in Fig. 7) have moderate

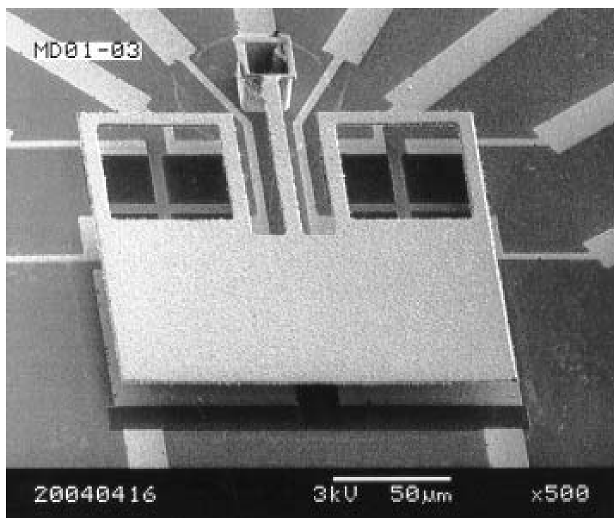

Fig. 7 – Scanning electron micrograph of a photodiode assisted closed loop light beam micromanipulator

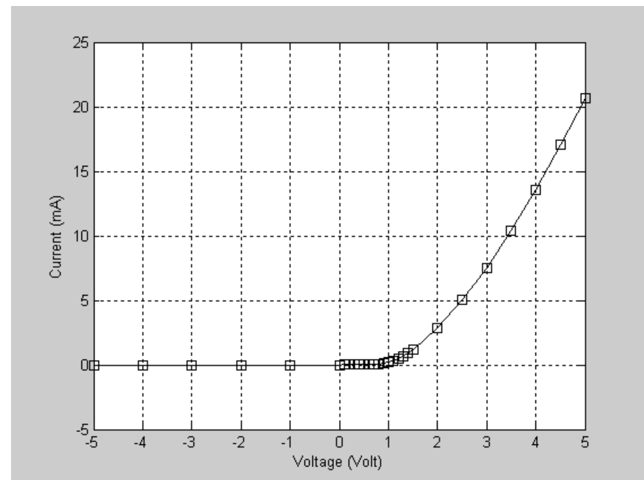

Fig. 8 – *I-V* characteristic of a photodiode element. The solid line is provided as visual aid.

planarity. This feature is being addressed in the second iteration microfabrication.

A number of randomly selected devices have been diced and packaged for characterization. The *I-V* characteristic of a photodiode element recorded in the absence of light is shown in Fig. 8. The dark current was measured to be ~ 4 μA for a reverse bias of 5 V. This relatively large value may be attributed to control of cleanliness during doping process or defects in insulating Si_3N_4 layer. The measurement of flexural deflection was performed for a range of actuation voltages. Incident light at wavelength of 0.63 μm was obtained from a 10 mW HeNe laser source. The incident power was adjusted through a variable attenuator and then focused on the manipulator. The latter was actuated using a square wave modulation from 0 to 15 V at frequency of 10 Hz. The deflected beam was directed to a linear position sensitive detector by means of a beam splitter. The deflection angle was computed from the beam position offset as determined with the use of the detector. Figure 9 compares the measured φ (V) characteristic with those obtained from the analytical and finite element modeling. The behavior of the experimental data is seen to be consistent with the modeling results. However, discrepancies in the required actuation voltage suggest that the actual value of the beam's Young modulus may be smaller then anticipated. In effect, the experimental and predicted pull-in voltages were respectively 17, 25, and 36 V. The discrepancy observed between the data computed analytically and by finite element modeling may result from the various assumptions made in the analytical derivation. In order to investigate the feedback mechanism, the variation of photocurrents with deflection angle was measured. During

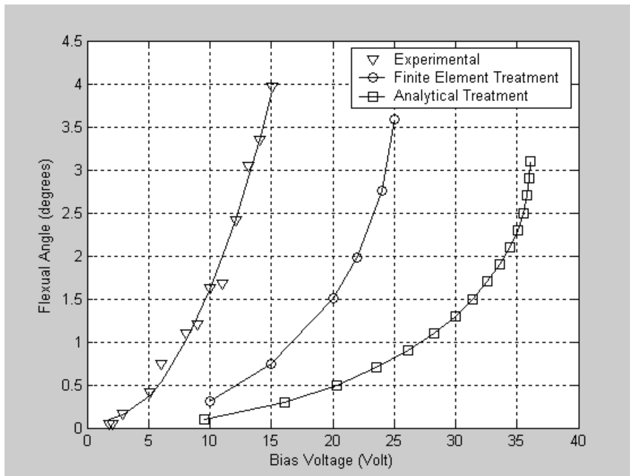

Fig. 9 – Experimental and predicted flexural deflection angles as a function of bias voltage. The solid lines are provided as visual aid.

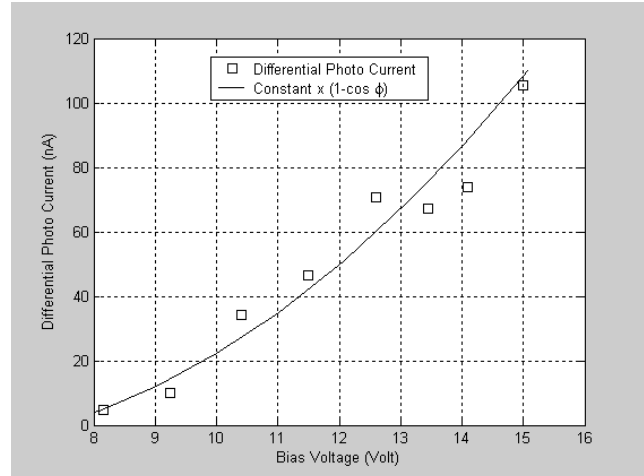

Fig. 10 – Differential photocurrents as a function of bias voltage. The solid line depicts the theoretically predicted (1-cosφ) dependence.

the experiment, the photodiodes were reversely biased at 5 V. The photocurrents generated from two vertically contiguous photodiodes were fed to a differential transimpedance amplifier and their difference was measured as a function of bias voltage. Referring to Fig. 2, the difference in photocurrent is seen to be proportional to the shaded area A_s and is therefore dependent on (1-cosφ). The values of (1-cosφ) were extracted as a function of bias voltage from the experimental data of φ (V) of Fig. 9 and then plotted in Fig. 10. The consistency obtained between the voltage dependence of differential photocurrent and the theoretical prediction demonstrated the effectiveness of the feedback mechanism.

6. Conclusions

We reported on an integrated feedback mechanism devised for flexural tortional devices. It consists in using monolithically embedded photodetectors to measure the portion of incident light crossing an aperture created in the manipulator. The manipulator position is determined from the detector section shadowed by the displaced aperture. A model was presented for the electrostatically actuated manipulators, predicting effects of structural parameters on angular displacement and resolution. As proof of concept, photodiode assisted closed loop manipulators were microfabricated in varying configurations on Si wafer. Their characteristics of deflection versus actuation voltage were found to be better than those predicted by the model. The feedback mechanism was validated in light of the consistency between differential photocurrents measured from contiguous photodiodes and theoretical prediction.

References

[1] H. Saito, T. Hashimoto, K. Kasamura, and H. Goto, *Proc. 13th AIAA-USU Conf. on Small Satellites* (1999).
[2] K. Petersen, *IBM J. Res. Develop*. 24, 631 (1980).
[3] P. Bandera, *Proc. 8th European Space Mechanisms and Tribology Symposium*, 61 (1999).
[4] H. Toshiyoshi and H. Fujita, *J. Microelectromechanical Syst.* 5, 231 (1996).
[5] J. Lee, L. Ngo Phong, and W. Zheng, *Technical Report*, Canadian Space Agency (2004).